European Research Infrastructure supporting Smart Grid Systems Technology Development, Validation and Roll Out

Technical Report TA User Project

onPDnet

Grant Agreement No:	**654113**
Funding Instrument:	**Research and Innovation Actions (RIA) ï Integrating Activity (IA)**
Funded under:	**INFRAIA-1-2014/2015: Integrating and opening existing national and regional research infrastructures of European interest**
Starting date of project:	**01.11.2015**
Project Duration:	**54 month**

Contractual delivery date:	**28/09/2018**
Actual delivery date:	**28/09/2018**
Name of lead beneficiary for this deliverable:	**Santiago Gonzalez, Haefely Hipotronics**
Deliverable Type:	**Report (R)**
Security Class:	**Public (PU)**
Revision / Status:	**released**

Project co-funded by the European Commission within the H2020 Programme (2014-2020)

Document Information

Document Version: 1

Revision / Status: released

All Authors/Partners Saliha Abdul Madhar, Haefely Hipotronics
Santiago González, Haefely Hipotronics
Peter Mraz, Haefely Hipotronics

Distribution List Santiago González, Peter Mraz, Saliha Abdul Madhar (Haefely)
Iñaki Orue, Sonia Barrios, Nabil Akroud, Ian Gilbert (OCT)

Document History

Revision	Content / Changes	Resp. Partner	Date
1	First version of report	Haefely	28.08.2018

Document Approval

Final Approval	Name	Resp. Partner	Date

Disclaimer

Copyright Notice

Table of contents

Abbreviations

PD	Partial Discharge
TA	Trans-national Access
onPDnet	Online Monitoring of Partial Discharges in Distribution Networks
HFCT	High Frequency Current Transformer
HF	High Frequency
LF	Low Frequency
BW	Bandwidth

Executive Summary

Asset management is one of the key strategies identified within Europe and globally for electricity networks particularly for the physical infrastructure of the assets, which are subject to regular maintenance programs. The advent of the smart grid has meant that these maintenance programs have developed from ‘reactive’ to ‘proactive’ and further to ‘predictive’, although the latter is still in its embryonic stages.

Partial discharge (PD) measurements provide as a good indicator of early stage problems with electrical infrastructure assets. Measuring and on-line monitoring of PD are being accepted more and more and in some cases becoming a standard practice in the maintenance programmes of network operators. The standards and characteristics of measuring equipment and procedures in laboratory environments is very well defined in their relevant standards, but in the field, the situation is extremely different and in-situ, in-service measurements have many other factors to consider.

Key areas of proposed research are:

- Network interaction in 3-phase cable systems
- Frequency response of various network configurations
- Full Bandwidth measurements with High Frequency Current Transformers (HFCT).
- Effectiveness of defect location in real networks.

The flexibility of the UDEX laboratory allows for the configuration of a real distribution network fulfilling the requirements of the proposed research areas.

The TA action has provided Haefely with free access to a laboratory, which may not otherwise have proceeded. The UDEX laboratory has a fully-operational distribution network for the purposes of research and Haefely, being an instrument manufacturer, has benefited from learning crucial features for PD measurement such as network interactions in underground cables.

Principal conclusions from the work carried out are:

- The attenuation of the higher frequency components of a PD pulse has been demonstrated through this research
- The utilization of the HF resonant components in the measured PD pulse allow a greater SNR but do not provide real value of charge.
- Applicability of the IEC 60270 measurement standards are relevant only while creating the test arrangement but bear no correlation while performing on-line measurements. Because calibration at frequencies lower than 100 kHz brings in very high levels of noise.

Lessons learned:

- The possibility of precise measurements with wideband sensors improves sensitivity at the cost of requiring more complex filtering and interpretation of acquired signals.
- Piecewise modelling of the complete network is vital for the development of calibration tools for the purpose of online PD monitoring.

General Information of the User Project

USER PROJECT	
Acronym	**onPDnet**
Title	**Online Partial Discharge measurements in real distribution networks**
ERIGrid Reference	**04.005-2018**
TA Call No.	**4th Call**

HOST RESEARCH INFRASTRUCTURE			
Name	**UDEX**		
Country	**Spain**		
Start date	**03/09/2018**	**Nº of Access days**	**15**
End date	**21/09/2018**	**Nº of Stay days**	**19**

USER GROUP	
Name (Leader)	**Santiago González**
Organization (Leader)	**Haefely**
Country (Leader)	**Switzerland**
Name	**Saliha Abdul Mahar**
Organization	**Haefely**
Country	**Switzerland**
Name	**Petr Mraz**
Organization	**Haefely**
Country	**Switzerland**

1 Research Motivation

Asset management is one of the key strategies identified within Europe and globally for electricity networks particularly for the physical infrastructure of the assets, which are subject to regular maintenance programs. The advent of the smart grid has meant that these maintenance programs have developed from ‘reactive’ to ‘proactive’ and further to ‘predictive’, although the latter is still in its embryonic stages.

Partial discharge (PD) measurements provide as a good indicator of early stage problems with electrical infrastructure assets. Measuring and on-line monitoring of PD are being accepted more and more and in some cases becoming a standard practice in the maintenance programmes of network operators. The standards and characteristics of measuring equipment and procedures in laboratory environments is very well defined in their relevant standards, but in the field, the situation is extremely different and in-situ, in-service measurements have many other factors to consider.

1.1 Objectives & Scope

Key areas of proposed research are:

- Network interaction in 3-phase cable systems
- Frequency response of various network configurations
- Full bandwidth measurements with High Frequency Current Transformers (HFCT).
- Effectiveness of defect location in real networks

2 State-of-the-Art

Asset management and the tools required for this activity are growing in importance for network operators. Indeed, in Europe, investment in R&D in this area has been identified as key for the future of networks [1]. Among the many different tools available for asset management of networks and components is online partial discharge (PD) measurement and monitoring [2-5].

Partial discharges (PD) can be precursors of failure and for this reason the presence and activity of PD is an important criteria for the condition assessment of insulation systems of electrical equipment. PD pulses ignite defects in insulation and cause macroscopic-physical effects, such as dielectric losses, electromagnetic transients, pressure waves, sound, light, heat and chemical reactions. For insulation condition assessment, these effects are measured with different kinds of sensors and the results will give information about insulation defects. The analysis of this information will provide information about the condition of the insulation. Therefore, the different PD detection methods can be regarded as an important diagnostic tool for non-destructive tests of insulation systems. Besides the conventional electrical PD detection in compliance to IEC 60270 [6], different non-conventional techniques are also used for both detection and location [7].

Techniques include:

- *Conventional Methods [IEC 60270]* : Integration of the frequency domain (either narrowband or wideband); and Integration in the time domain (wideband)
- *Non-conventional methods*: Detection of electromagnetic transients (HF/VHF or UHF); detection of acoustic emission; detection of optical occurrences; analysis of chemical compounds.

The main non-conventional methods used for detection and localization of PD defects are the electromagnetic HF (3MHz ï 30MHz) / VHF (30MHz ï 300MHz) / UHF (300MHz ï 3GHz) and the acoustic PD detection.

Such techniques are not only used for off-line and on-line PD diagnosis tests under on-site condition but also for quality assurance tests in laboratory.

Conventional PD measurement uses the apparent charge, which is the integrated current pulse, caused by a PD, flowing through the test circuit. The conventional method allows a precise calibration, and requires a sufficient signal-to-noise ratio of the measurement circuit to easily discern the PD in question. The standardized method of IEC-60270 and AC test protocol is well established for factory and laboratory testing, but is often not appropriate for on- site testing. In the case of field-testing where very high background noise levels are present, non-conventional methods with high signal to noise ratio capabilities are the best way to obtain meaningful measurements.

It is this very point that this proposal wishes to address, highlighting the differences in methodology requirements for laboratory and field based PD measurements and their interpretation ï especially in light of the growing use of data analytics in the smart grid towards automation of asset management systems (implicitly requiring suitable data).

3 Executed Tests and Experiments

The test plan and set-ups were as set out in the following subsections.

3.1 Test Plan

WEEK 1	03.09.2018	Preliminary information on UDEX configurations
	04.09.2018	Detailed planning
	05.09.2018	preliminary calibration
	06.09.2018	Test using HFCT+Haefely Detector
	07.09.2018	On-line test (problems with PD from source)
WEEK 2	10.09.2018	Problem solved , Installation of Elec. measurement
	11.09.2018	Test 1
	12.09.2018	Test 2
	13.09.2018	Test 2
	14.09.2018	Test 3
WEEK 3	17.09.2018	Test 3
	18.09.2018	On-line test with real defect + Workshop
	19.09.2018	On-line test with real defect
	20.09.2018	On-line test with real defect
	21.09.2018	Test repetitions

3.2 Test Setups and Methodology

3.2.1 TEST 1: 3-PHASE CROSS COUPLING

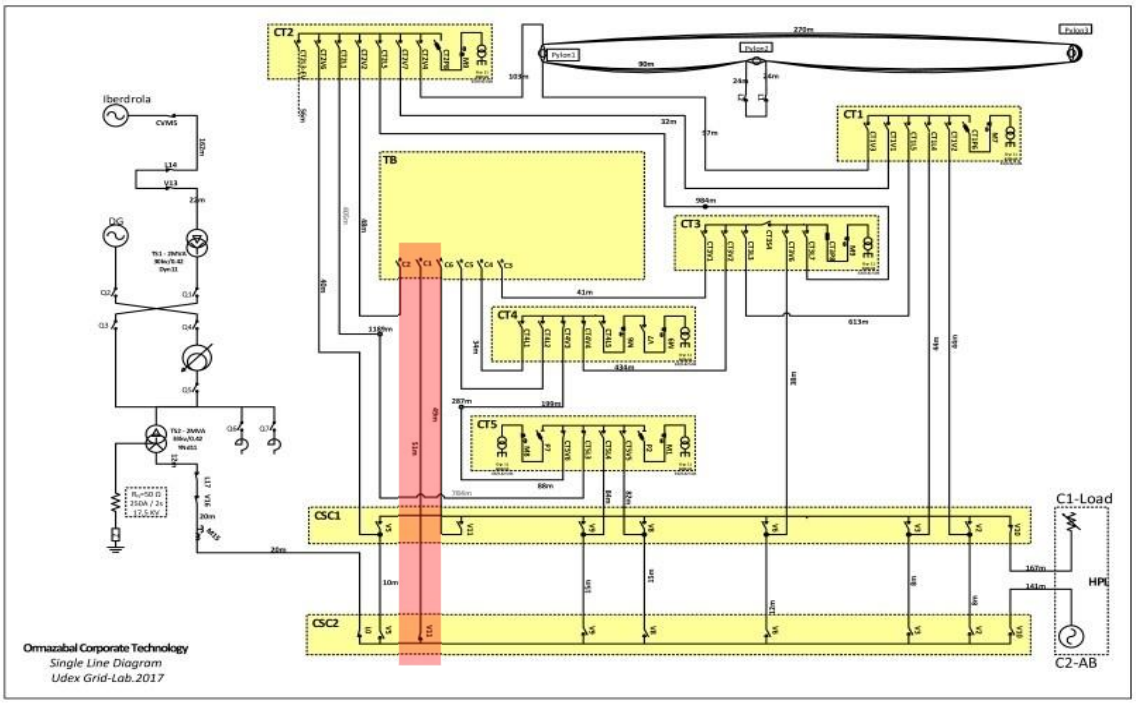

CASE A: Cable grounds connected together on injection end

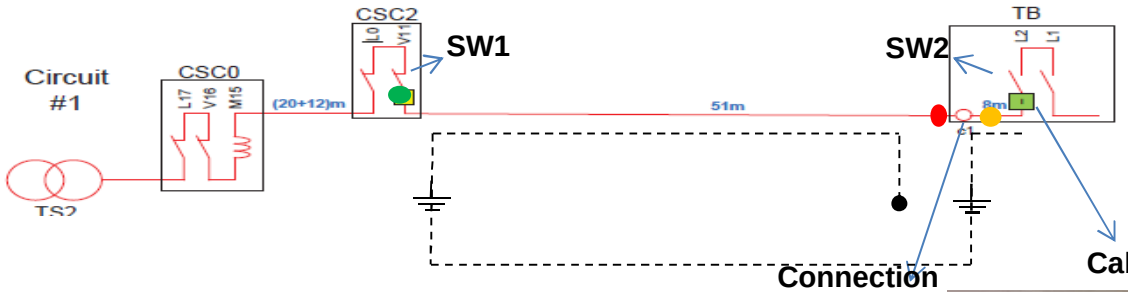

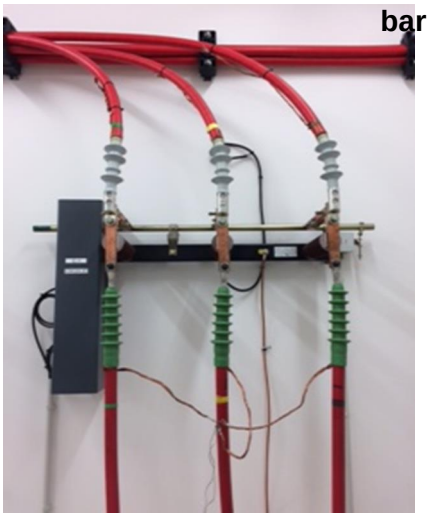

Pre-requisites:

- SW1 is open
- SW2 is open

Procedure:

- Calibration pulse is injected over Phase 1 (P1) at CSC2 ●
- 3 PD detectors are connected at TB ● over P1, P2 and P3 to measure cross-coupling between phases.
- Using an oscilloscope record the individual pulses at each of these phases and obtain FFT (with and without Analog Filter ON)
- Include the HFCT at the measuring point with the Coupling capacitor and AKV still connected and using the oscilloscope record the individual pulse and obtain the FFT.
- Remove the AKV and repeat step 4.

CASE B: Cable grounds connected separated physically (repeat same procedure of Case A)
These measurements should ideally measure the pulse propagation just through the cable with no coupling to other phases due to absence of any physical connection amongst them.
However, some cross-coupling is expected sue to the physical proximity of the cables that can be considered as a stray capacitance.

CASE C: Cable ground sheath interrupted (repeat same procedure as Case A)
These measurements are designed to learn the effect of interruption in the cable earth connection.
The measurement point is shifted to the other side of the connection bar. ●

3.2.2 TEST 2: NETWORK INTERACTION

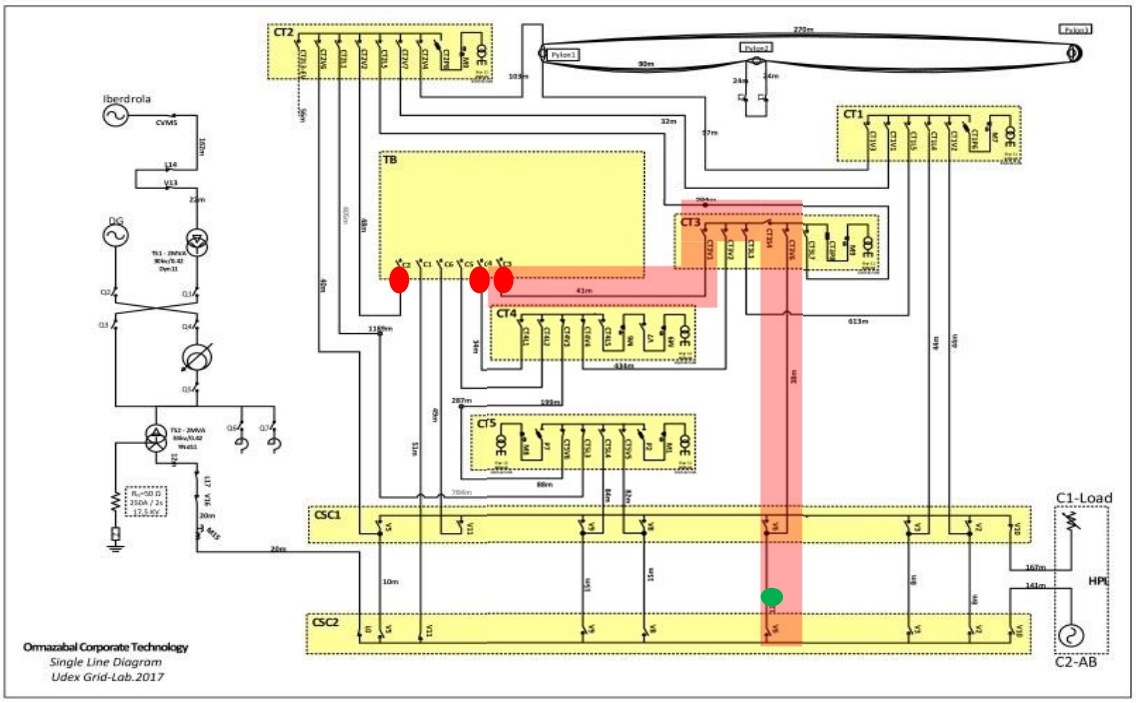

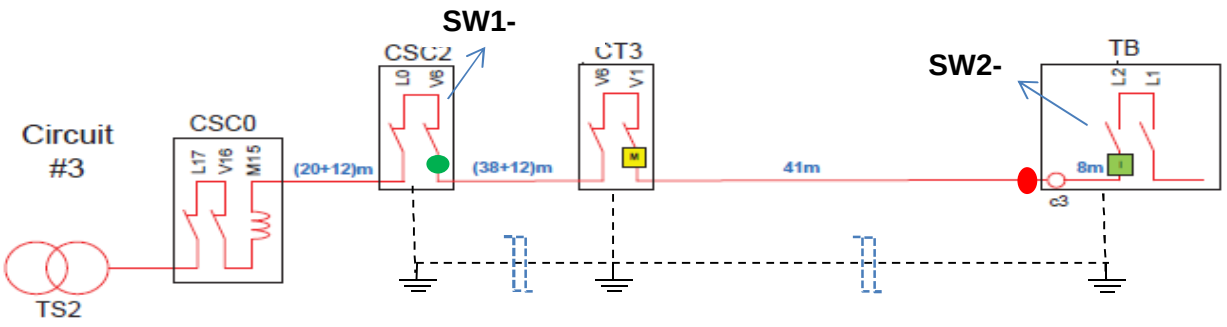

Note:
Substation CT3, busbar CSC2 and the test bay (TB) have a common ground therefore it is expected that any pulse that is injected at CSC2 appears at TB first through the coupling via the ground connection.
The cable ground connection is interrupted at point C3.

CASE A: Pulse transmission through a substation with common ground
Procedure:

- Pulse is injected at CSC2
- Measuring at the TB: incoming cables from CT2, CT3, CT4 at the connection bar where the ground connections are left isolated.

*(Results to be recorded are the same as Test 1)

CASE B: Pulse transmission through a substation with isolated ground
(Same as Test2, Case A)

CASE C: Pulse injected at the Substation and measuring at both ends

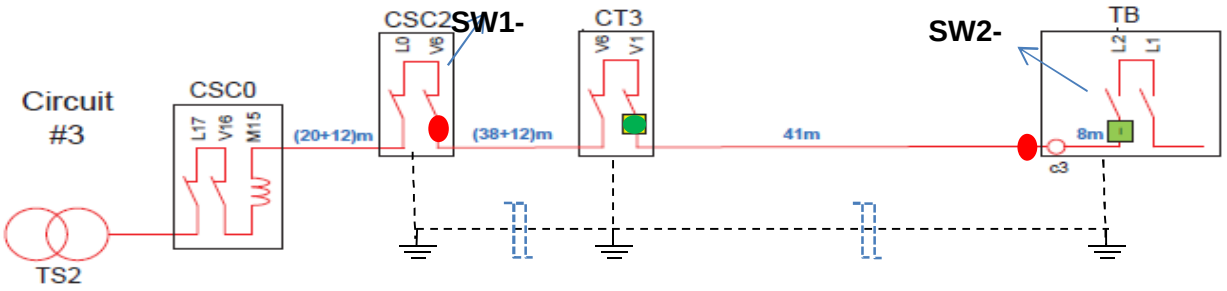

The cable lengths from CT3 to CSC2 and to TB differ only by 1 m. Hence, it is interesting the see the PD measurement at the 2 cable ends. Fault location of DDX can be used.

3.2.3 TEST 3: PD MEASUREMENT ON LONG CABLE WITH JOINTS

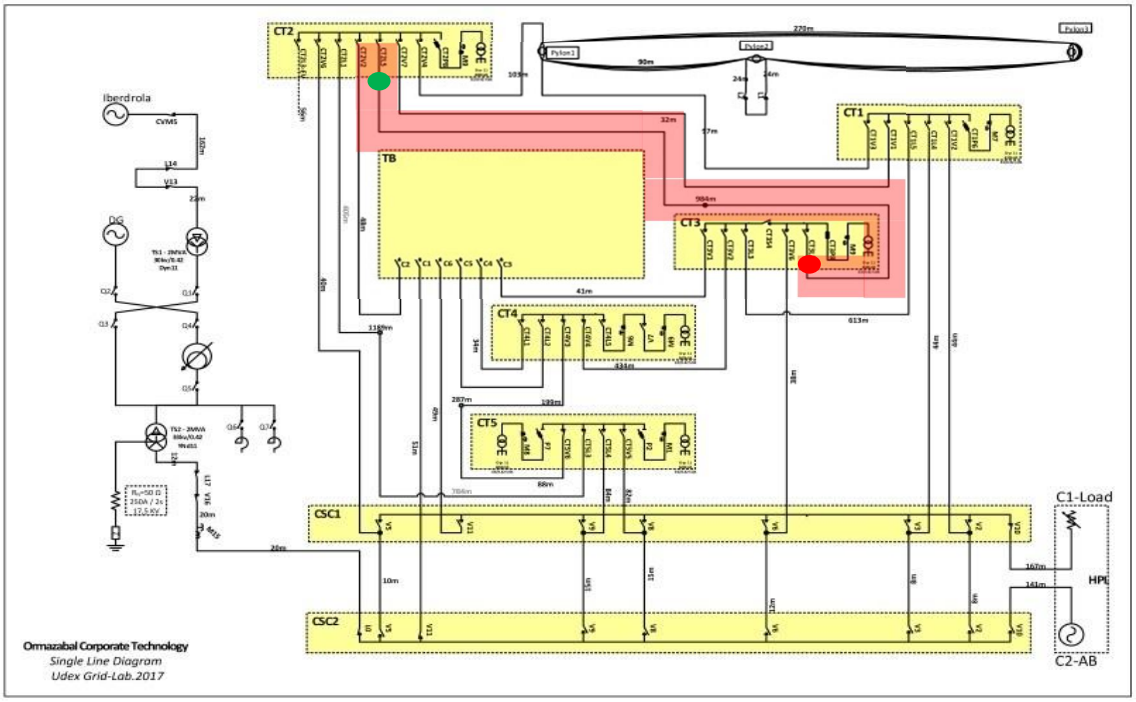

Sensitivity of AKV (IEC band) Vs HFCT can be compared over measuring on long cable length (1.153 km).

3.3 Data Management and Processing

The user group carried out all data acquisition and processing with their own equipment. Where possible, the host institution carried out measurements in parallel as a comparison.

4 Results and Conclusions

4.1 TEST 1: 3-PHASE TESTS ON SHORT CABLE LINK

The short cable link between the supply Busbar (CSC2) and the Test Bay (TB) measuring 51m in length is selected to perform the preliminary set of measurements to study the 3-phase coupling between lines and investigate the effect of different grounding configurations. The tests are performed using a calibrator (Haefely's KAL 9520) and High Frequency Current Transformers (HFCT100 from HVPD) for the measurement of the pulses.

4.1.1 Configuration 1

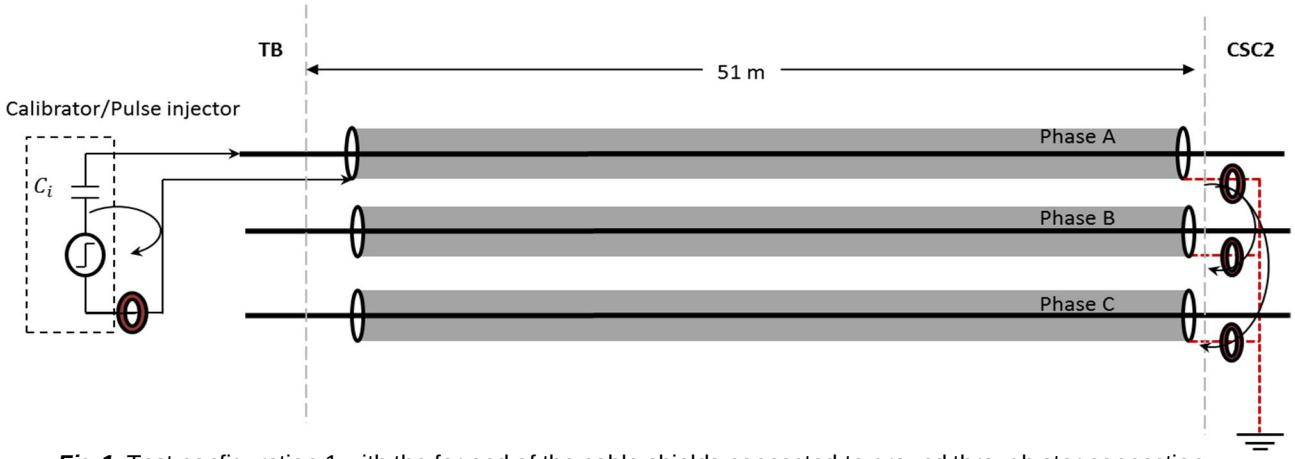

Fig.1. Test configuration 1 with the far end of the cable shields connected to ground through star connection.

The reflection coefficients at the near end (□) and far end (□) are calculated as follows;

□ □ □□ □ □□ □□ □ □□ □ 1 □□□□□□□□□□ □□□□ □□□ □□□□□ □□□□□□□□□□ □□. 3. □

□ □ 1 □□□□□ □□□□

Based on the calculated reflection coefficients the theoretical directions of current flow can be deduced as shown in Fig.1, these help us to verify the results of the measurements. The results of the measurement are shown in Fig.2. The results indeed verify the direction of the current flow deduced based on the reflection coefficients.

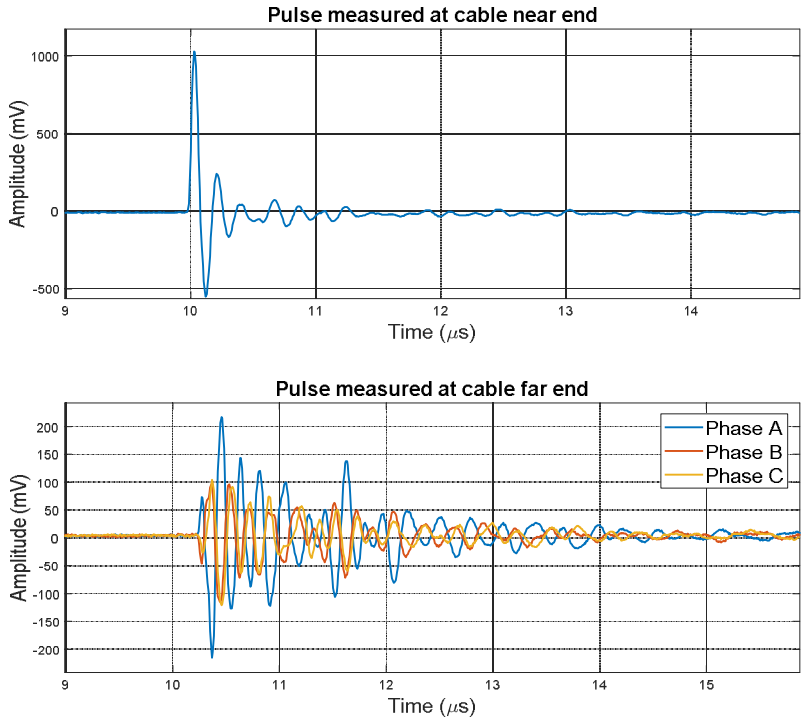

Fig.2. Pulses measured at the near end (top) on Phase A and at the far end (below) on all phases.

However, the short length of the cable makes it complex to isolate and identify the pulse reflection from the cable end (open end). Therefore, frequency analysis is employed to find the standing wave ratio in the cable section. The frequency spectrum of the measured pulses shown in Fig.2 are presented in Fig.3. The resonant peaks occur at 1.7, 3.4 and 5.2 MHz. These resonant peaks are an artefact of the measurement and arise from the standing waves in the cable due to non-homogenous impedance of the propagation path. This can also be calculated as follows;

$$\text{[illegible]}\ (\text{[illegible]}) = 51\ \text{[illegible]}$$

$$\text{[illegible]} = \frac{\text{[illegible]}}{\sqrt{\text{[illegible]}}} = \frac{\text{[illegible]}}{\sqrt{2.8}} \sim 170\ \text{[illegible]}/\text{[illegible]}$$

$$\text{[illegible]} = \frac{2\text{[illegible]}}{\text{[illegible]}} = 600\ \text{[illegible]} \rightarrow 1.7\ \text{[illegible]}$$

Therefore this proves the resonant peaks are not the energy of the pulse by itself but arise from the presence of a standing wave in the cable section. The resonances are at multiples of 1.7 MHz; 1.7, 3.4 and 5.2 MHz.

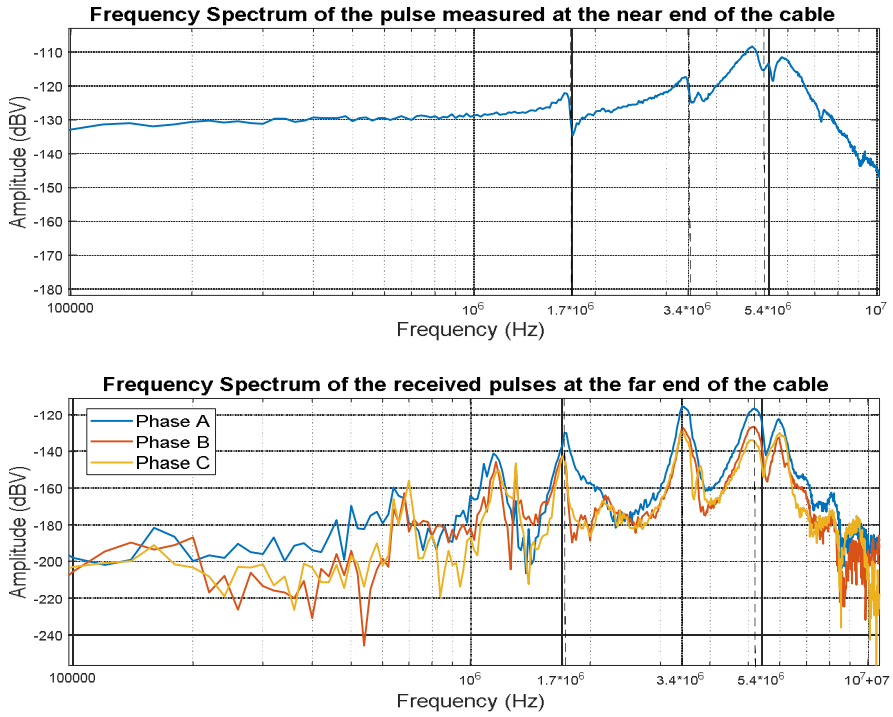

Fig.3. Frequency spectrum of the measured pulses presented in Fig.2.

Lastly, it is also interesting to note the amplitudes of the measured pulses on Phases A, B and C. The current of the pulse on Phase A should roughly be the sum of the current on Phases B and C, ignoring the stray coupling to the earth. The measured voltages can be translated to values of current through the transfer function of the HFCT which in this case is 4 mV/mA.

$$\frac{72.76}{4} \sim \frac{41.02 + 26.61}{4}$$

$$18.19 \sim 10.255 + 6.6525 \approx 16.9$$

$$\approx 1.29$$

4.1.2 Configuration 2

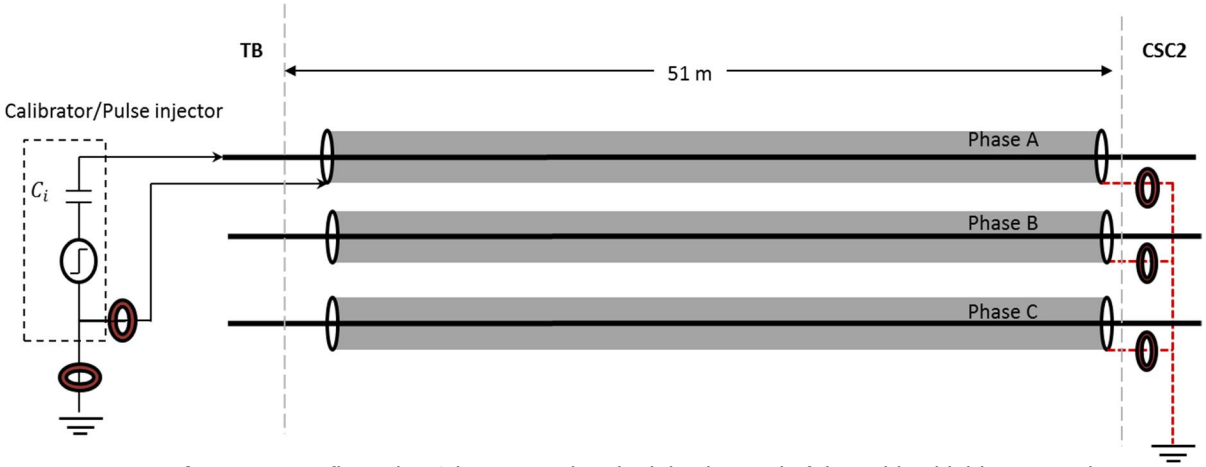

Fig.4. Test configuration 2 by connecting the injection end of the cable shield to ground.

The goal of this test configuration is to measure the fraction of stray coupling to the ground while injecting into a cable whose cable shield is grounded at the injection terminal. And indicate the differences in injection scenario when the cable shield at the point of injection is isolated from the ground and the influence it may have on the measurement.

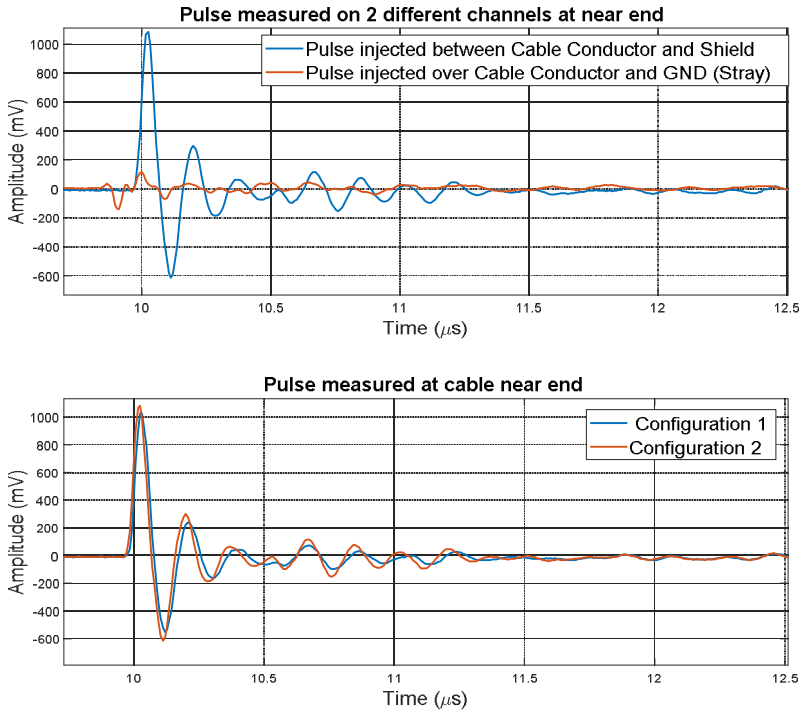

Fig.5. Pulse measured at the cable near end at 2 positions as indicated on Fig.4.

The pulse injected on the ground channel as a consequence of the parasitic capacitance is very meagre. The influence of the direct connection to ground of the cable shield at the injection terminal is also very insignificant. It can be expected that if the stray capacitance is large and in the order of magnitude of the cable capacitance, the influence will be greater. This is generally experienced in laboratories with a complete copper mesh beneath the floor which provides a high value of stray capacitance. This inference is drawn from the following relation derived using the equivalent circuit shown in Fig.6.

$$V_{inj} \propto \frac{C_{stray} \cdot C_{cable}}{C_{stray} \cdot C_{cable} + C_{cable} \cdot C_{inj} + C_{stray} \cdot C_{inj}} . 1$$

As long as the value of C_{stray} is several order of magnitudes smaller than C_{cable}, the charge injected will remain relatively constant.

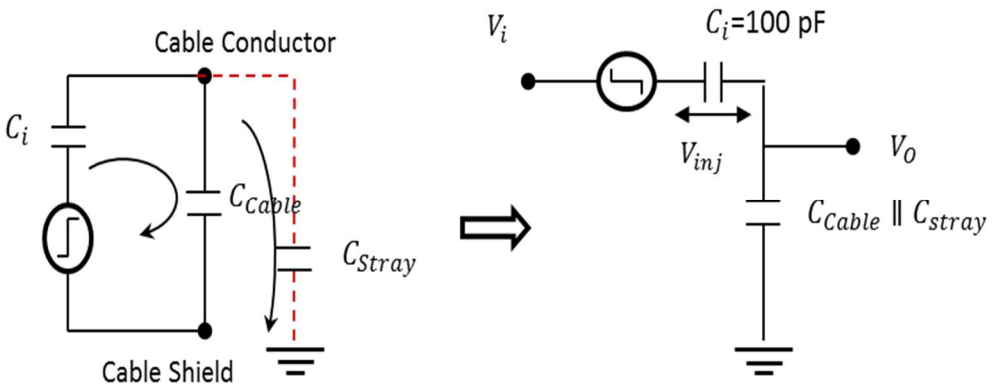

Fig.6. Equivalent circuit representation of the test case discussed in Section 4.1.2.

4.1.3 Configuration 3

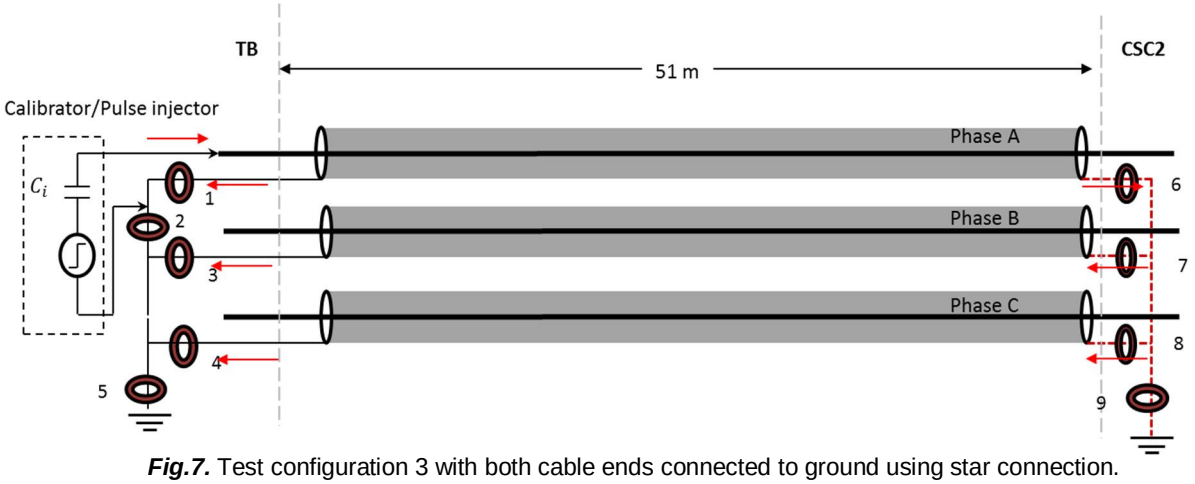

Fig.7. Test configuration 3 with both cable ends connected to ground using star connection.

The measurements are made at the locations indicated on Fig.7 in order to determine the current loops in the circuit and to draw an inference on whether such a connection influences the charge injection/measurement on a cable network, if so how.

The pulses measured at the injection end (at positions 1, 3 and 4) and their respective spectrum in the frequency domain are shown in Fig.8. Similarly the induced currents on the cable shields at the far end of the cable are shown in Fig.9. The ground return currents on Phases B and C are once again identical and their polarities have been utilised to derive the current direction in the circuit (indicated by the red arrows on Fig.7).

Based on the ratio of the currents on Phase A versus the currents induced on Phases B and C at the injection end of the cable it is determined that 1/30th of the current couples to the other phases via the parasitic capacitance.

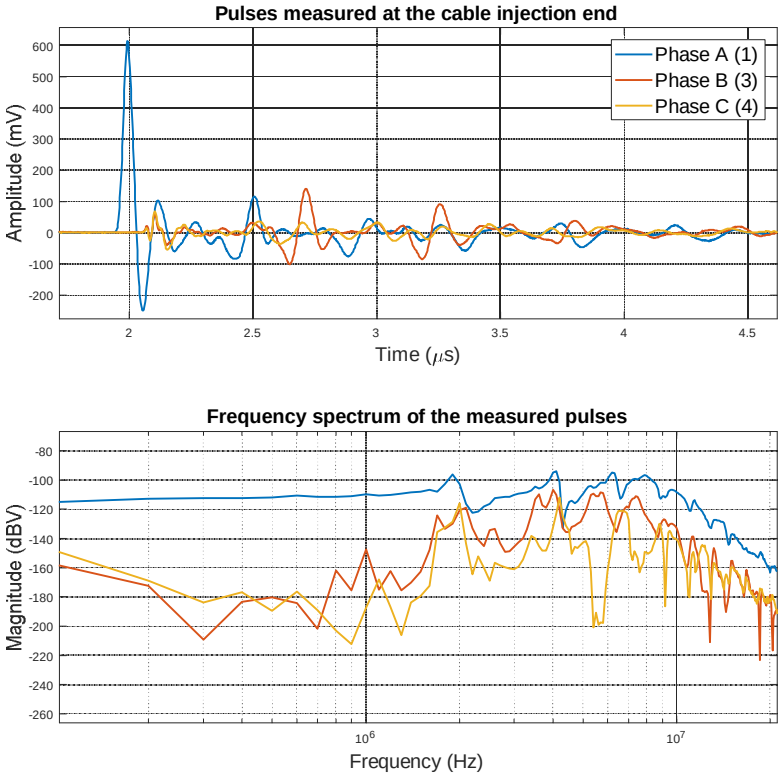

Fig.8. Pulses measured at the cable injection end in test configuration 3.

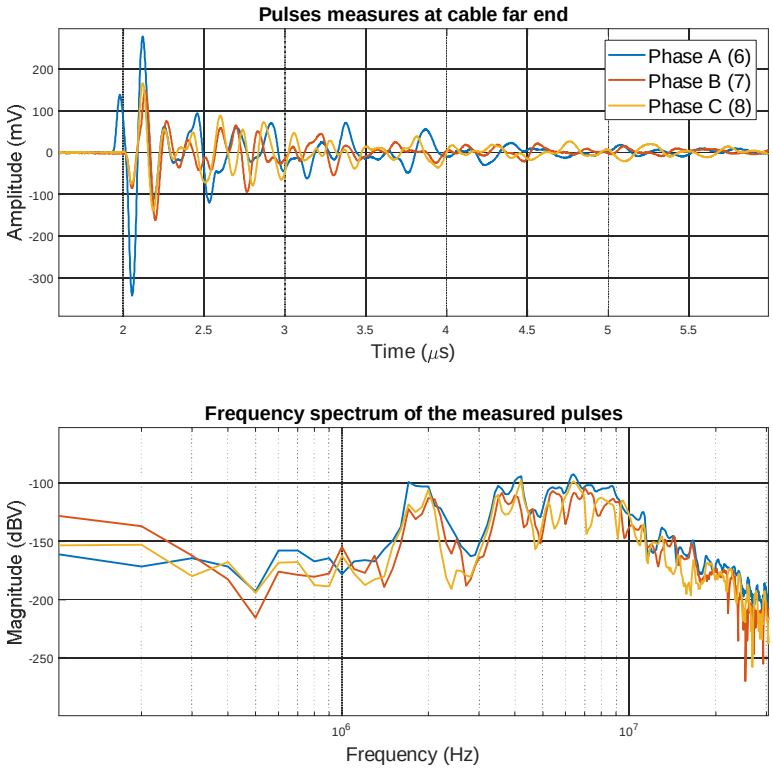

Fig.9. Pulses measured at the cable shield on the cable's far end (open) in test configuration 3.

From the following tests it can be concluded that there is no significant difference in using the different grounding configurations. However the direct connection to ground leads to the creation of a ground loop that brings in large ground noise at lower frequencies (~kHz up to 1MHz). Therefore it is recommended to use inductive grounding especially while making HF partial discharge measurements.

4.2 REAL DEFECT AT CABLE TERMINATION: WITH GROUND INTERRUPTION

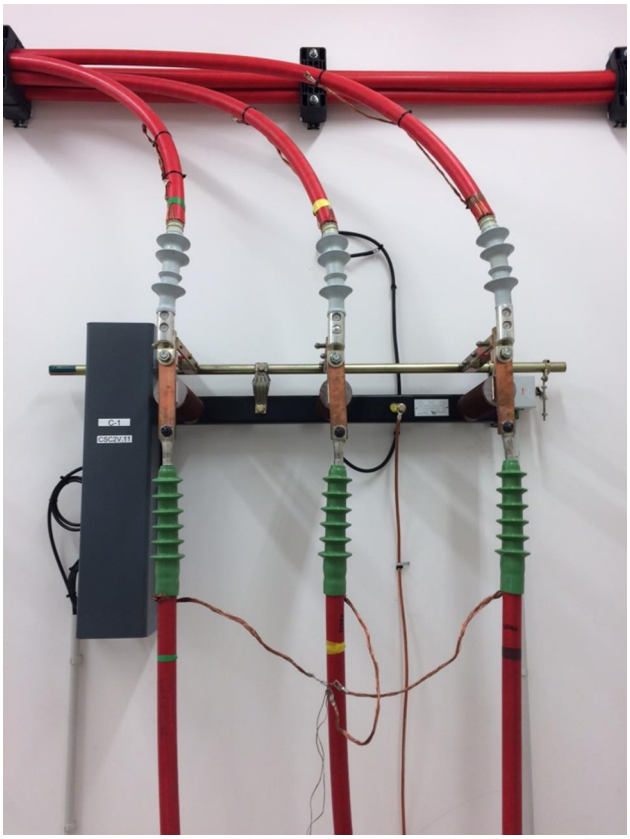

Fig.10. Grounding configuration used at the Test Bay (TB).

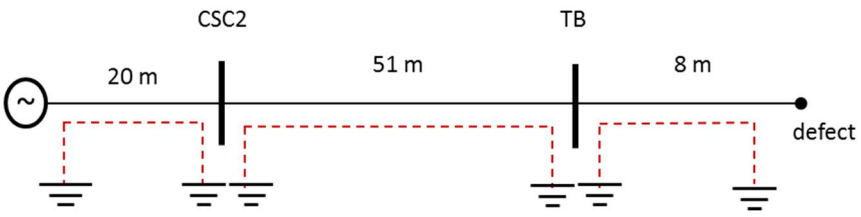

Fig.11. Single line diagram of the test case with real defect.

4.2.1 Measured using Coupling capacitor

The HFCT used for measuring the defect were connected on the 8m side of the cable shields. The cable shields themselves were connected together in a star connection going to ground. Once the whole circuit was closed, excluding the connection to supply, a final calibration was done at the TB to check the frequency response of the complete line. But before selecting the frequency BW for calibration the frequency spectrum of the noise is studied to determine if there are any unwarranted peaks that can be avoided. Fig.12 shows the noise spectrum on the connected line. And Fig.13

shows the pulse shape and the frequency spectrum of a 10 nC calibration pulse injected at the terminals of Phase A.

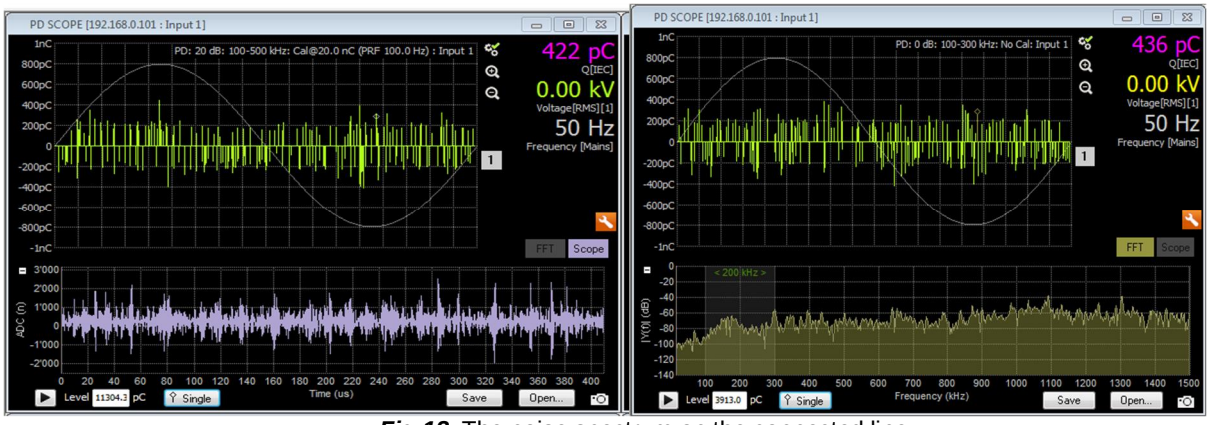

Fig.12. The noise spectrum on the connected line.

To perform a valid calibration it is vital to choose the correct bandwidth of measurement. Choosing the spectrum where the energy of the pulse is relatively flat/constant provides stable and linear charge measurements.

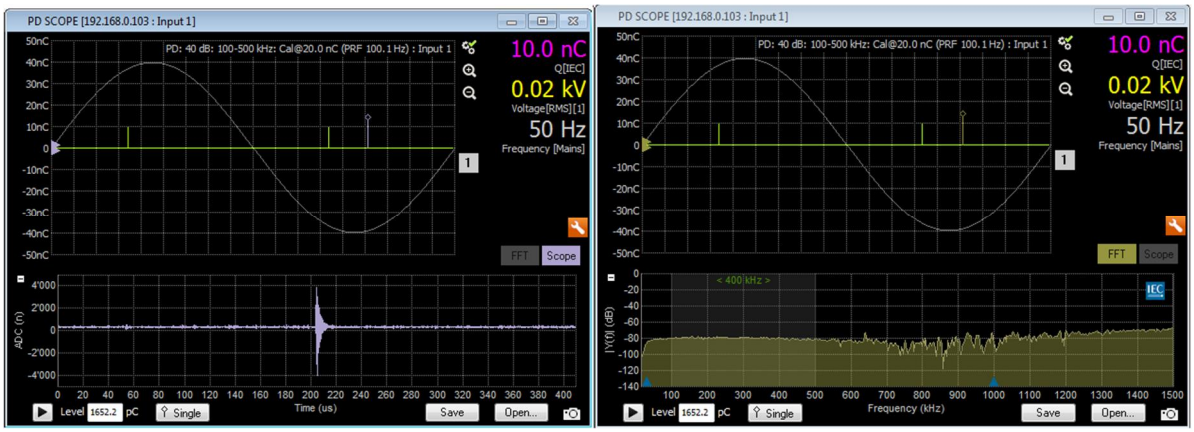

Fig.13. The calibration pulse and its spectrum as recorded using the DDX 9121b.

Moreover since the cable network is a one-dimensional system for a PD pulse propagation its frequency response analysis can be studied using a calibration pulse in order to check the wave velocity, points of reflection and so on. From Fig.14 resonant peaks can be seen at multiples of 1.7 MHz which is the frequency of the standing wave in the 51 m line.

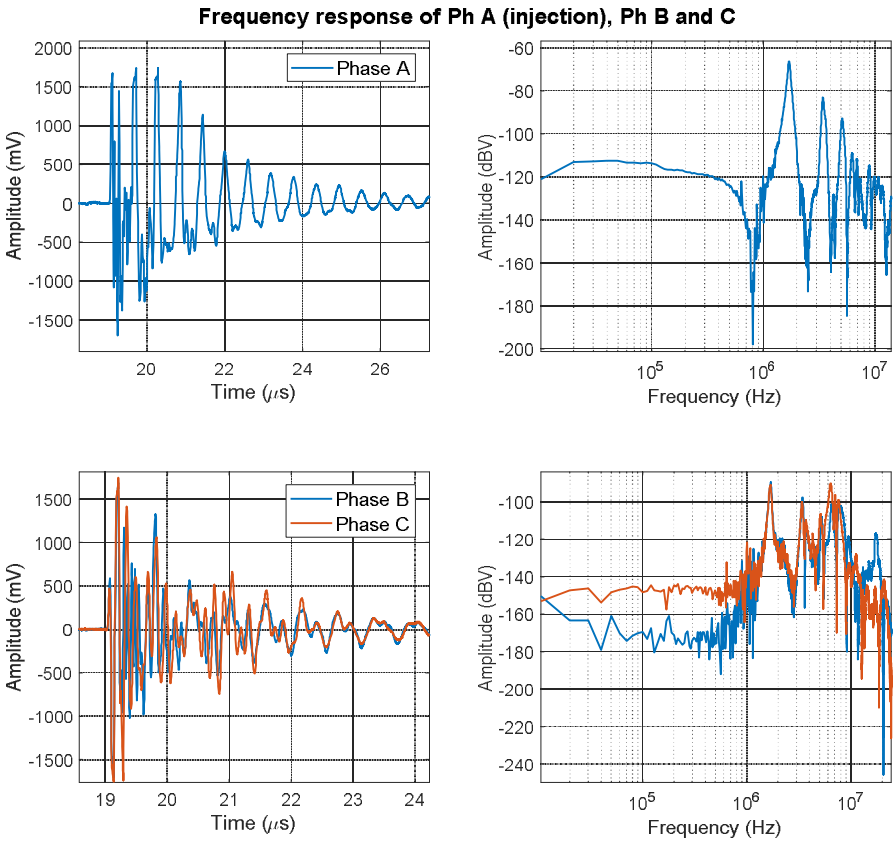

Fig.14. The frequency response of the injection Phase A and cross-coupling to other phases.

Fig.15 shows the frequency spectrum of the calibration pulse on Phase A and the spectrum of the cross-coupled pulses on phases B and C as recorded by the DDX 9121b. From the displayed value of charge it can be seen that the ratio of cross-coupling to the other 2 phases (healthy) is 13%.

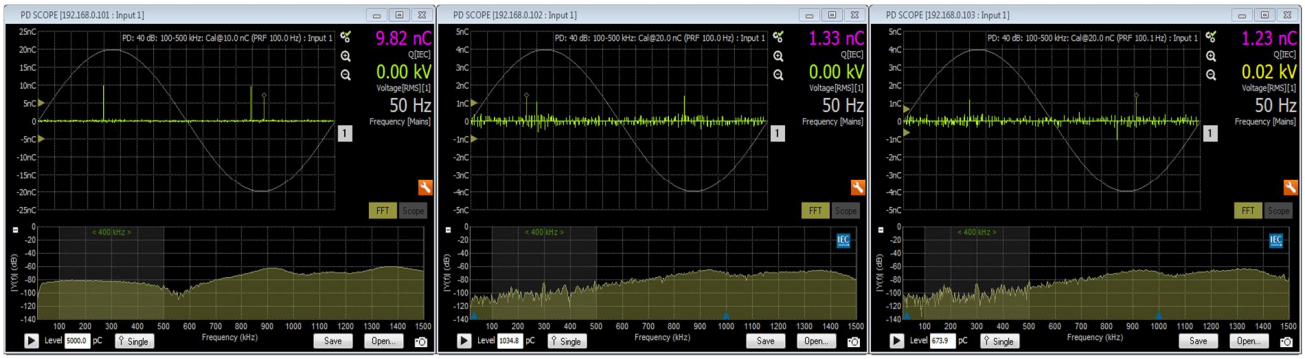

Fig.15. Frequency spectrum of the calibration pulse injected on Phase A (left) and cross-coupled on Phase B and C.

The defect inception occurs around 6 kV rms. Fig.16 shows the PRPD pattern recorded for the respective defect. The clusters on the negative axis on the positive half-cycle and the positive polarity on the negative half-cycle are the actual clusters that represent the defect from the floating potential. The other 2 are created due to unstable polarity recognition due to the highly oscillated nature of the discharge pulse. A short analysis is done also on the real discharge pulses measured on Phases A, B and C.

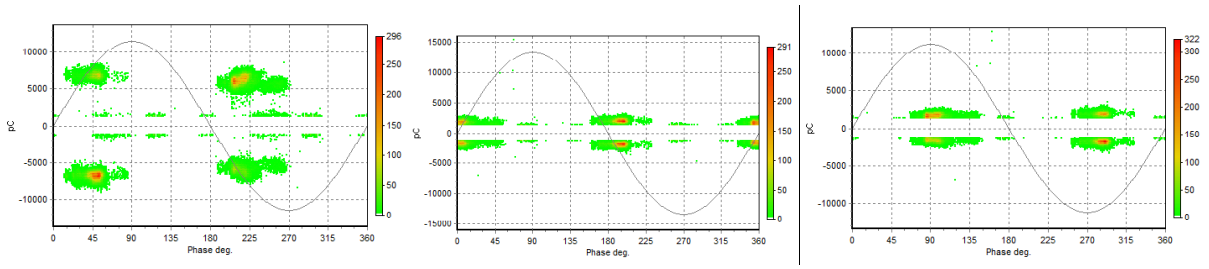

Fig.16. PRPD pattern recorded for Phase A (defective), Phase B and Phase C (healthy) using Ck.

From the frequency spectrum presented on Fig.17 it can be observed that the flat frequency spectrum occurs at lower frequencies (<400 kHz) and resonance peaks appear at higher frequencies. Indeed it will provide a greater sensitivity of measurement while measuring at higher frequencies but provides poor pulse discrimination since the resonances are dominant on all 3 phases, as they arise from the physical structure of the line. Thus, it is a trade-off between discharge sensitivity and accurate measurement.

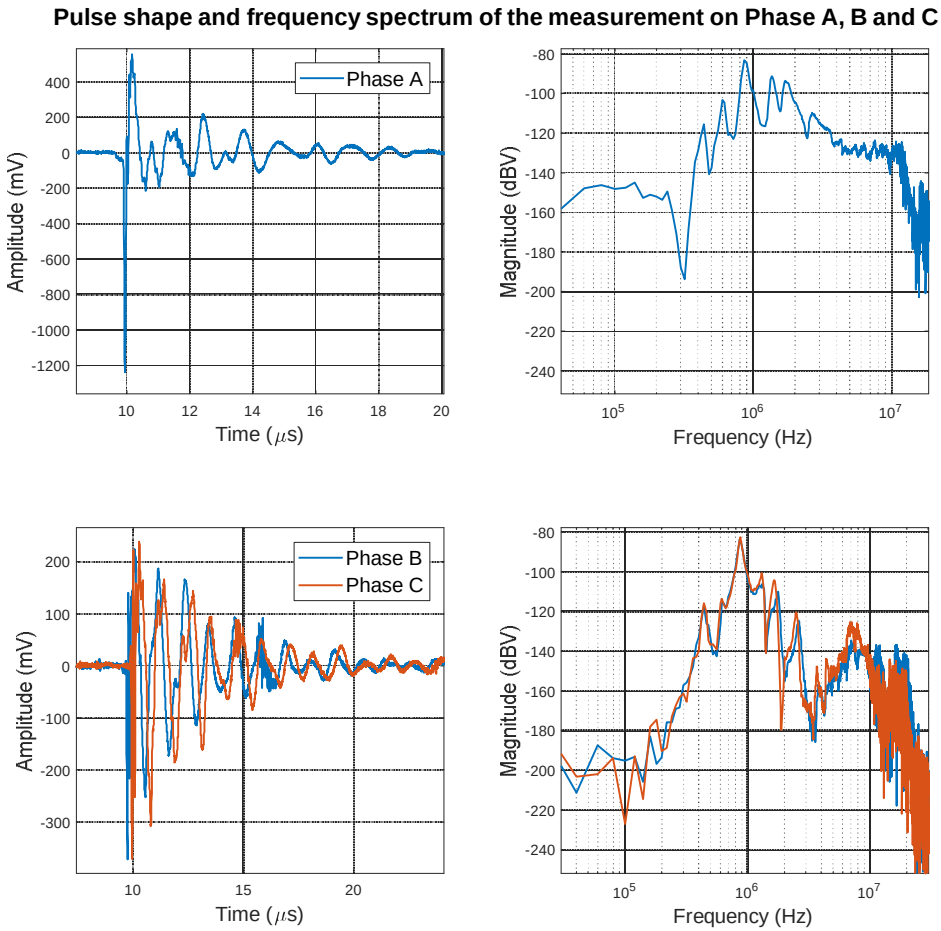

Fig.17. The pulse shape and frequency spectrum of the real discharge pulses measured on Phase A (defective), Phase B and C (healthy).

4.2.2 Measured using HFCT

The test with the real defect is repeated using the HFCT instead of the coupling capacitor. The

HFCT has a wide measuring bandwidth between 200 kHz and 19 MHz. So the measured pulses represented in this section are closest to the real/full bandwidth pulses we could measure.

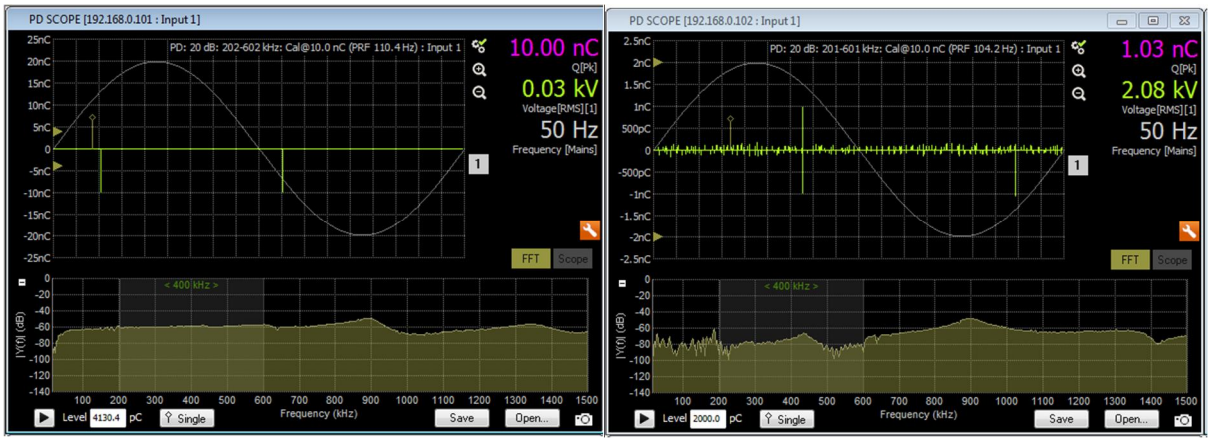

Fig.18. Frequency spectrum of the calibration pulse injected on Phase A (left) and cross-coupled on Phase B (right).

Fig.18 shows the spectrum of the calibration pulse that was injected on Phase A and the cross-coupled pulse on the other phase with its respective spectrum. Once again it can be noted that the flat frequency spectrum which represents the energy of the parent pulse is only at the lower frequencies. The higher energy that prevails in the higher frequencies is not from the high frequency components of the pusle but from the pulse overlapping that is a consequence of pulse reflections from discontinuities on the propagation path.

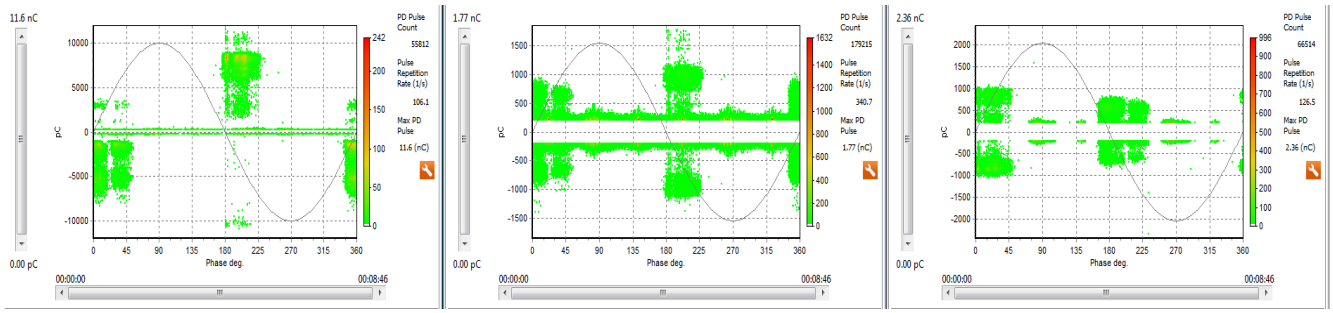

Fig.19. PRPD pattern recorded for Phase A (defective), Phase B and Phase C (healthy) using HFCT.

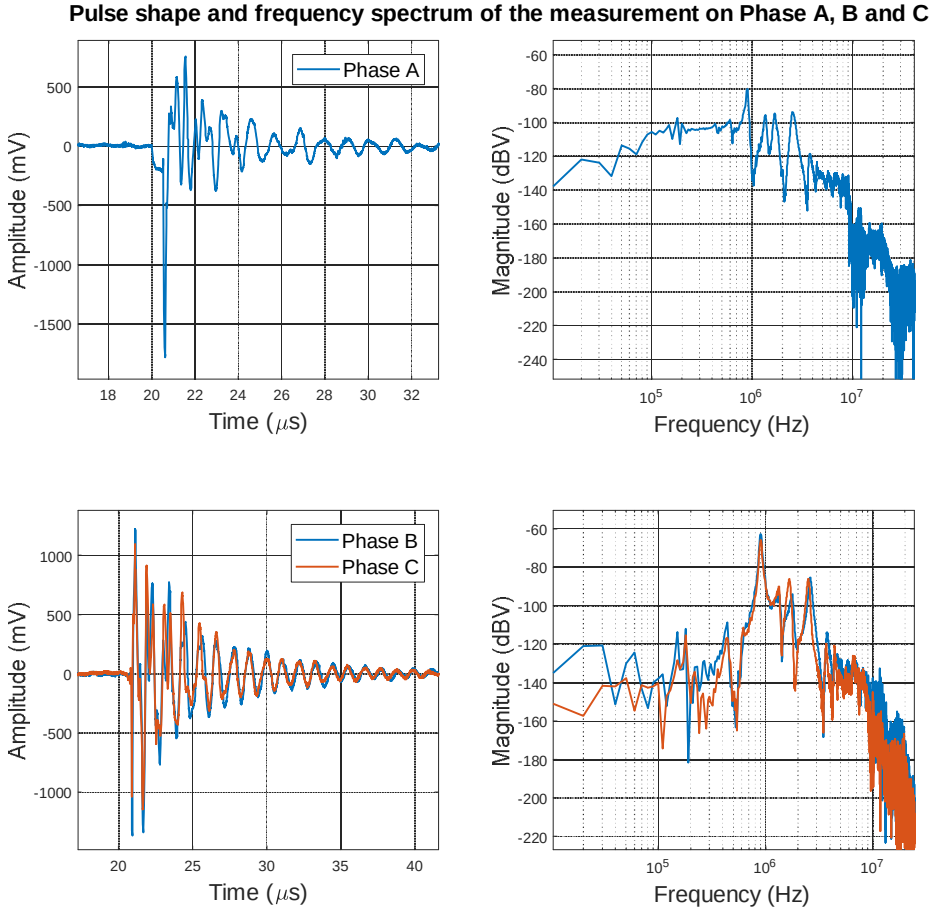

Fig.20. The pulse shape and frequency spectrum of the real discharge pulses measured on Phase A (defective), Phase B and C (healthy).

The detector is calibrated with the HFCT as measurement impedance in the frequency bands (200-600 kHz). The PRPD pattern recorded by the detector is presented in Fig.19. It can be observed that the pulse recognition is fairly stable and there is no double recognition of the pulse due to the oscillations. This is because of calibration at the low frequency band limits the large pulse oscillations. This can be seen through Fig.21 which shows the full bandwidth pulse and the bandwidth limited pulse along with their corresponding frequency spectrums. It shows that the majority of the pulseôs energy lies at the LFs and the information at the HFs brings no useful information. It is in many cases more advantages to make a BW limited measurement to make the pulse recognition more stable. Further this brings several advantages such as defect identification through pattern recognition.

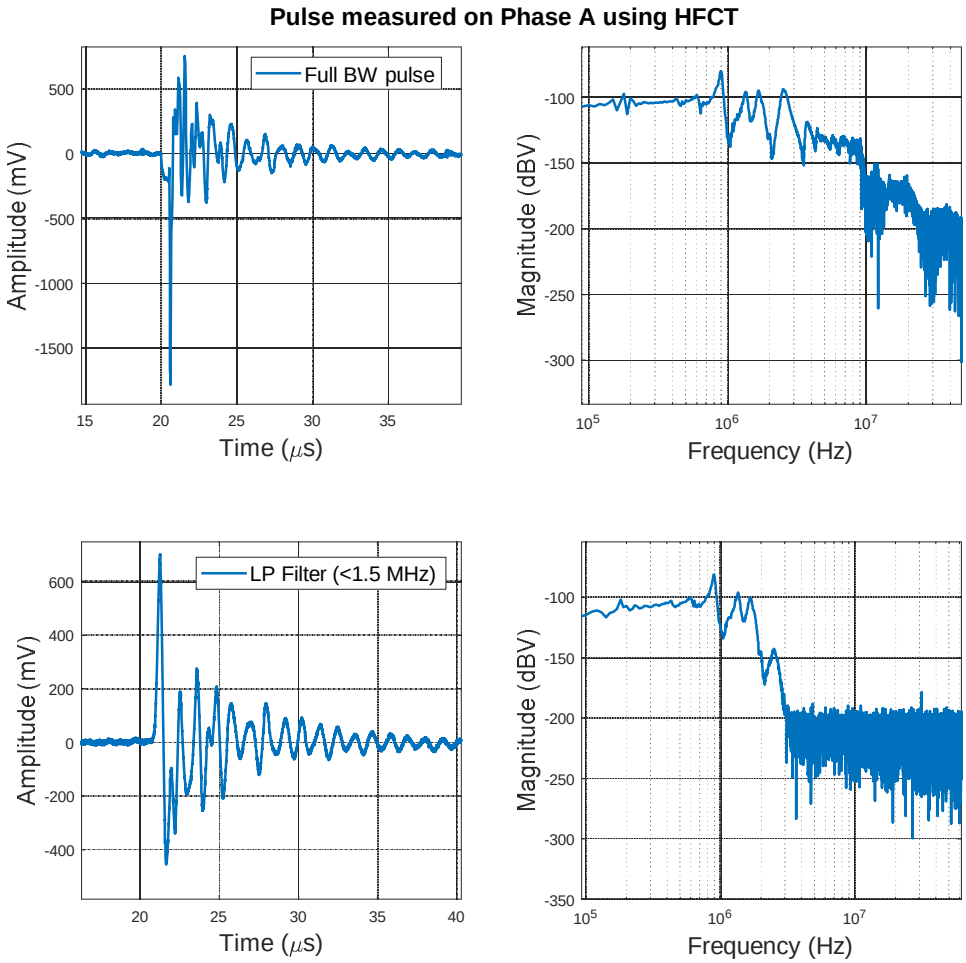

Fig.21. The discharge pulse on Phase A and its frequency spectrum as measured using the HFCT.

4.3 REAL DEFECT AT CABLE TERMINATION: WITH CONTINUOUS GROUND

Fig.22. Ground configuration at the Test Bay (TB).

When the ground connection of the cable is made continuous it is observed that the travelling pulse is less damped and therefore a higher sensitivity is achieved. Fig.23 shows the cable's response to a 10 nC calibration pulse firstly measured between conductor and ground (as discussed in the previous section) and next by measuring between conductor and cable shield using a coupling capacitor. The differences in the amplitude of the measured pulse can be well observed. In addition, the low frequency (<1 MHz) components are well preserved in the second case which can be inferred from the well-defined frequency spectrum.

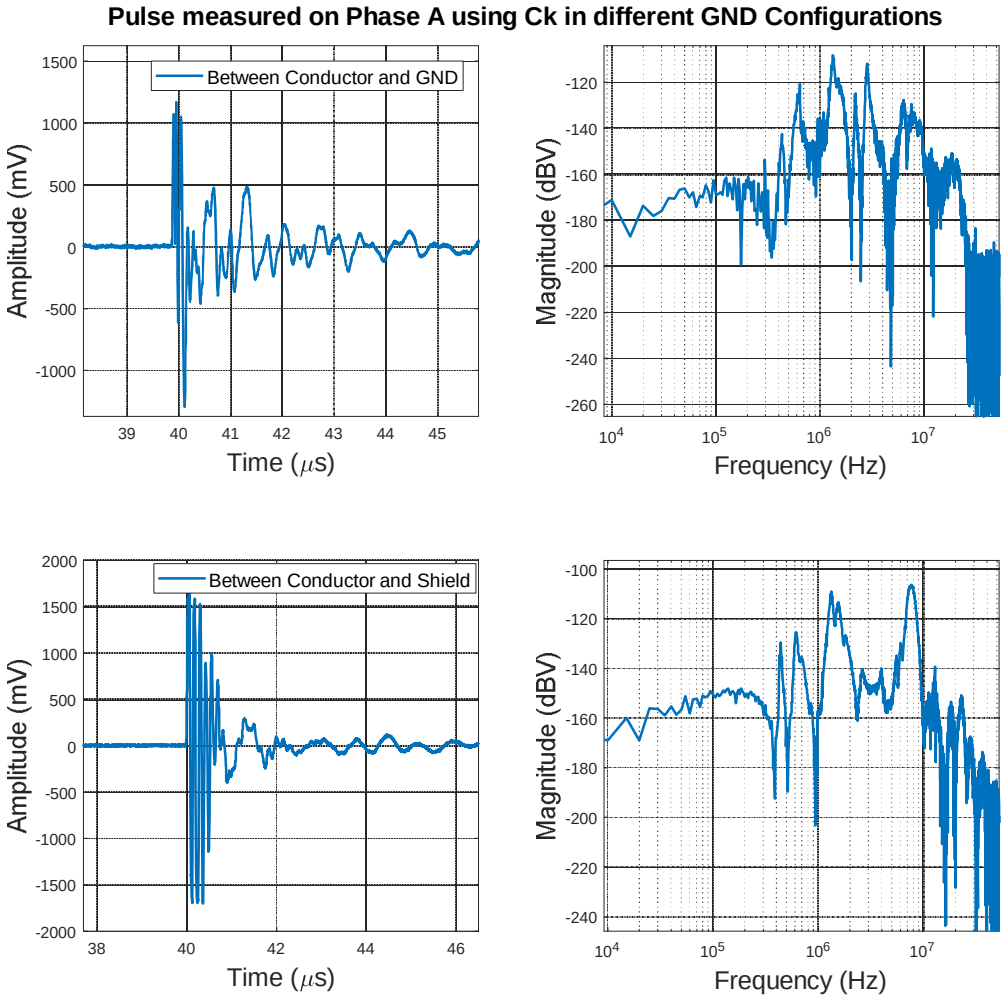

Fig.23. The pulse frequency response of 2 different ground/measurement configurations discussed.

4.4 NETWORK INTERACTIONS IN UDEX

The network configuration used to study the interactions via interconnections, ground-loops and radiation is shown in Fig.24. The various test cases are presented sequentially in this section.

4.4.1 Case 1: Injection and measurement at CT2 (TB)

The injection and measurement over the same terminal allows us to deduce the velocity of pulse propagation over the propagation channel from the pulse reflection from the far end of the cable, usually left open. It can also help provide an impression of the attenuation of the partial discharge pulse with propagation over long distances.

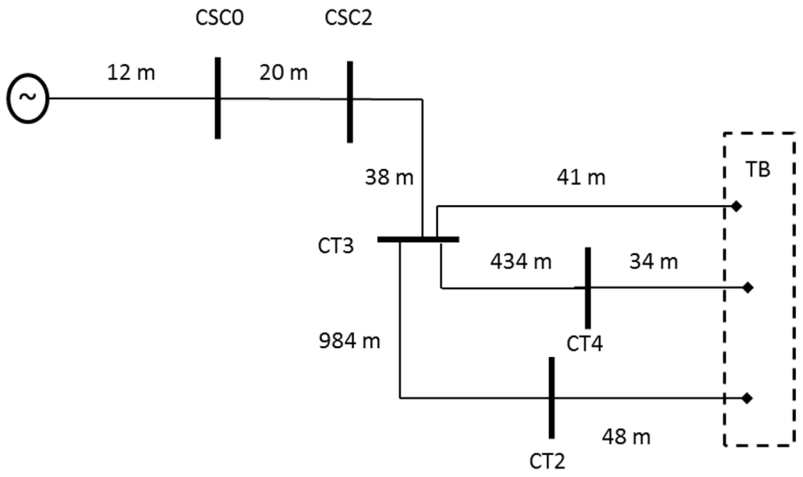

Fig.24. Network configuration used for the tests performed in Section 4.4.

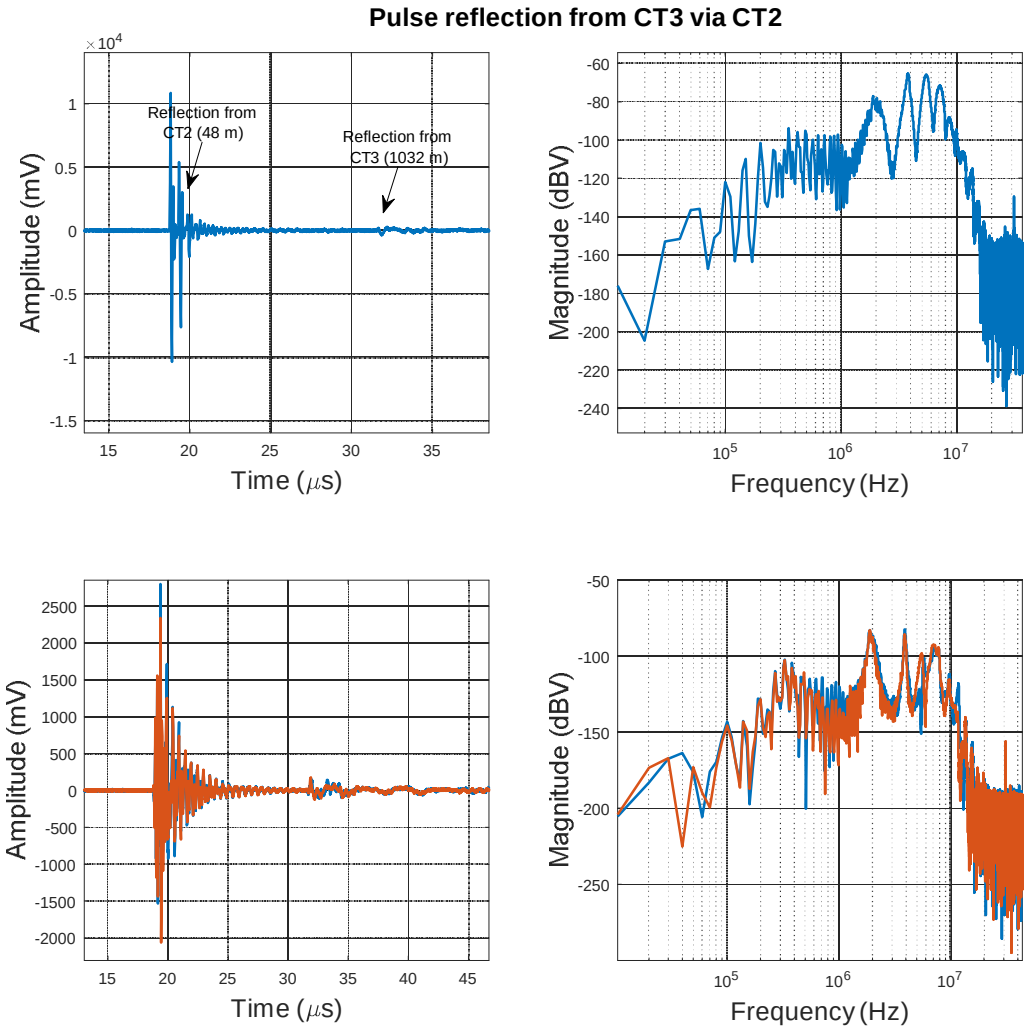

Fig.25. The pulses measured at the cable near end at CT2 (TB) and their frequency spectrums.

□□□□□□□□ □ 2□/□ □ $\frac{\square\square\square\square\square\square\ \square}{\square\square.\square\square\ \square\square}$ □ 167 □/□□

4.4.2 Case 2: Injection at CT3 (TB) and measurement at CT2 (TB)

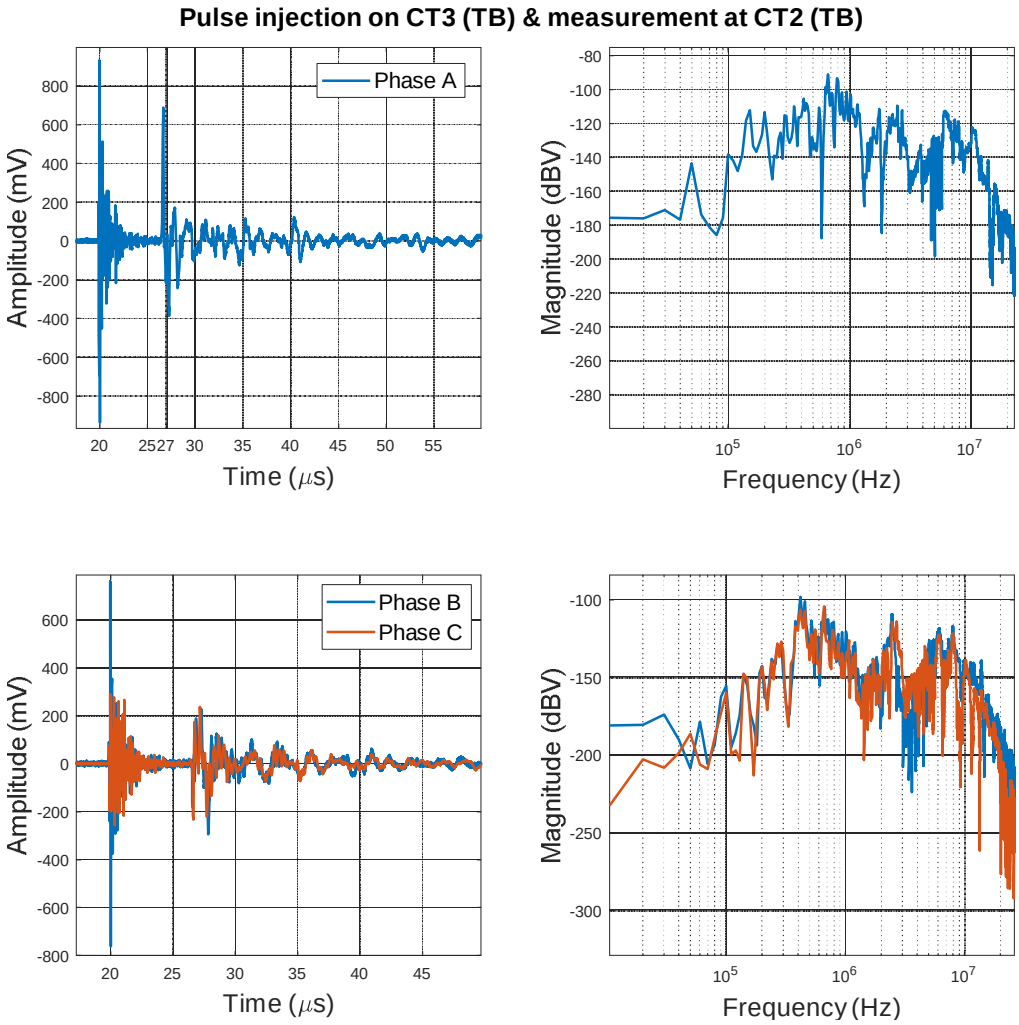

Fig.26. Pulse injected at CT3 (TB) and measured at CT2 (TB).

In Fig.26 it can be observed that a HF pulse precedes the actual discharge pulse. This is the pulse coupled directly to the measuring setup from the injection loop, radiated through air. This is because all the cable terminals exit at the Test Bay and it is practically impossible to isolate one of the lines. This was also investigated and the frequencies at which the pulse radiatively couples to the measuring loop are the same frequencies that are present on the HF pulse on Fig.26.

4.4.2.1 Measurement with Real defect

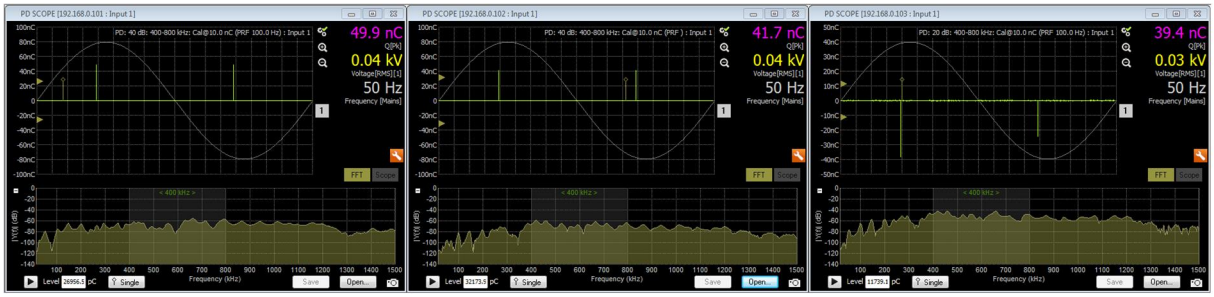

Fig.27. The spectrum of the calibration pulse injected on Phase A of CT3 and received at CT4

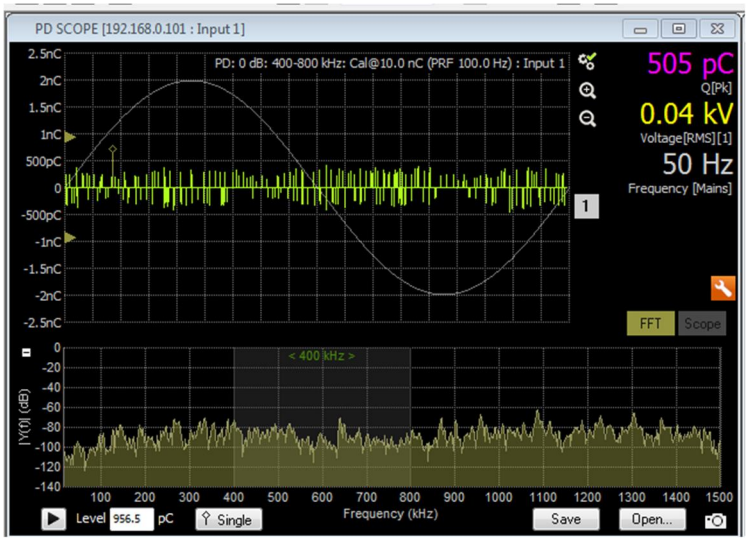

Fig.28. Noise spectrum after calibration

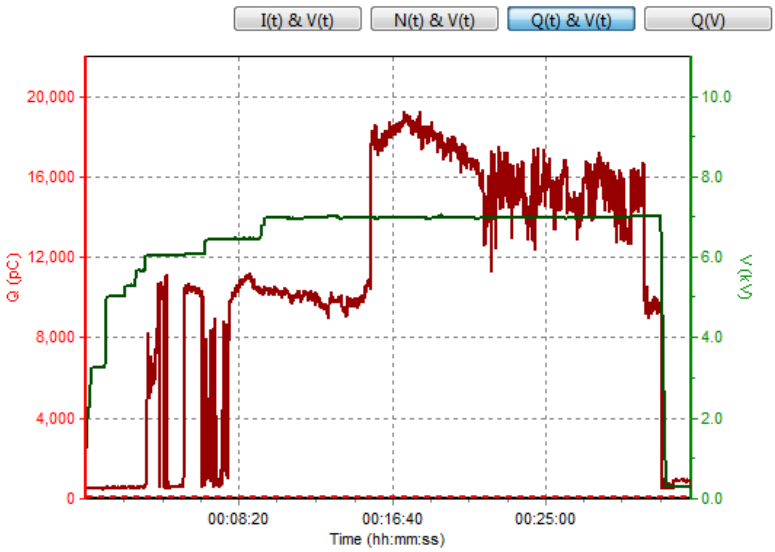

Fig.29. The Charge Vs Time plot for Phase A of the Test Case.

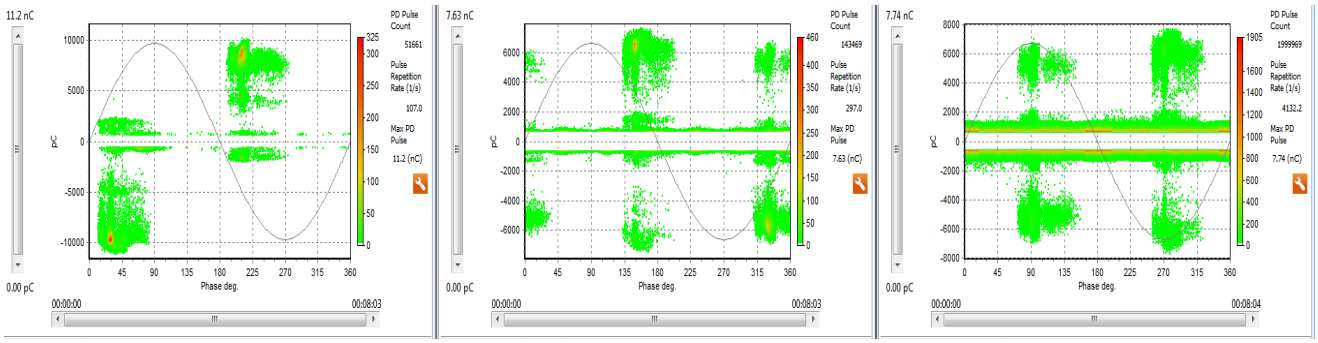

Fig.30. PRPD pattern recorded on CT2 (TB) with defect at CT (3).

The real defect is connected to CT3 and connected to the branched network configuration going through CT4 and CT2.

4.4.3 Case 3: Injection at CT3 (TB) and measurement at CT4 (TB)

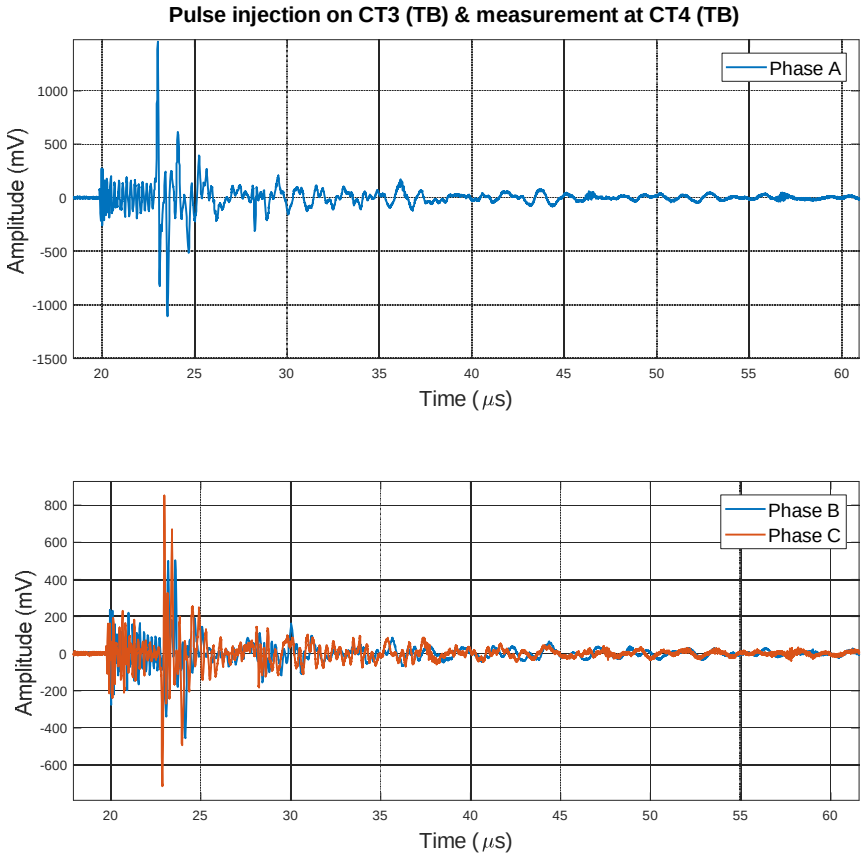

Fig.31. Pulse injected at CT3 (TB) and measured at CT4 (TB).

4.4.3.1 Measurement with Real defect

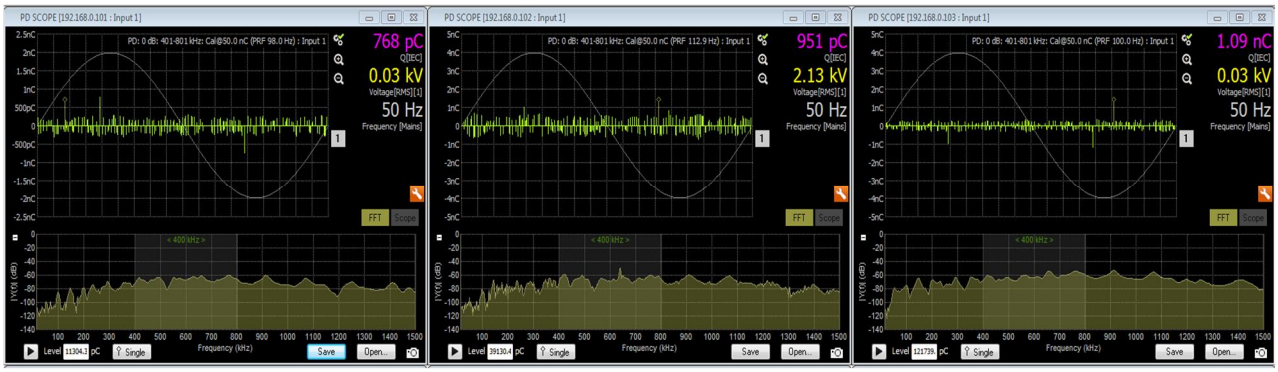

Fig.32. The spectrum of the calibration pulse injected on Phase C of CT3 and received at CT4

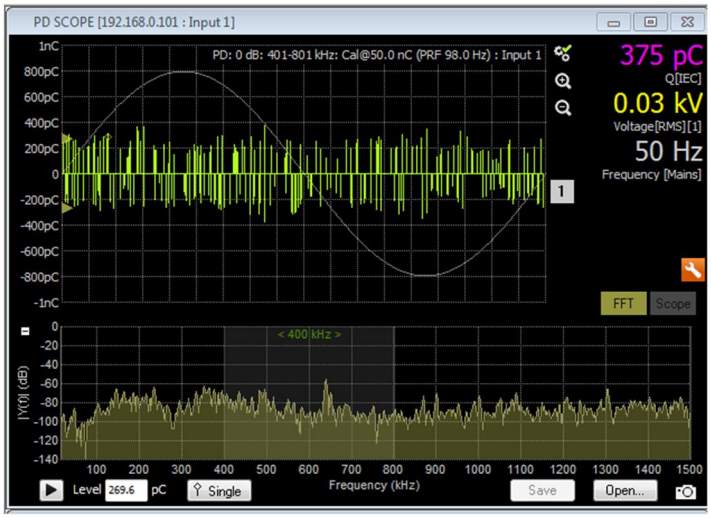

Fig.33. Noise spectrum after calibration

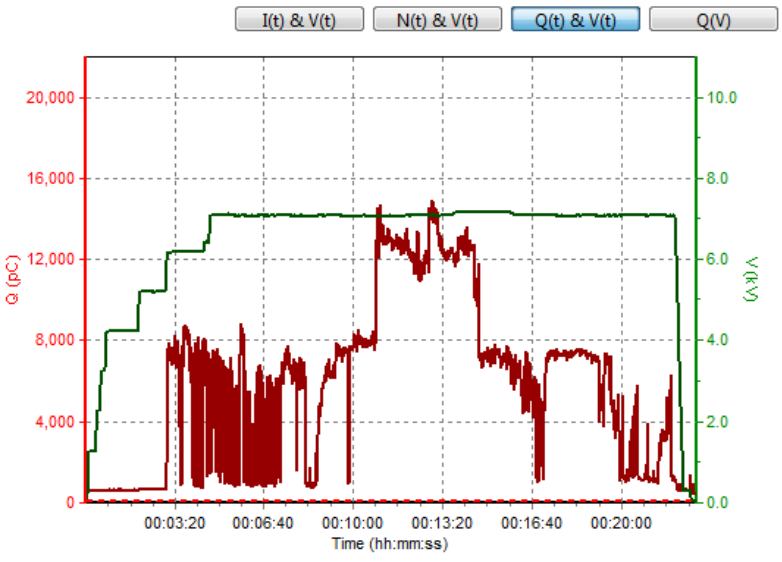

Fig.34. The Charge Vs Time plot for Phase A of the Test Case.

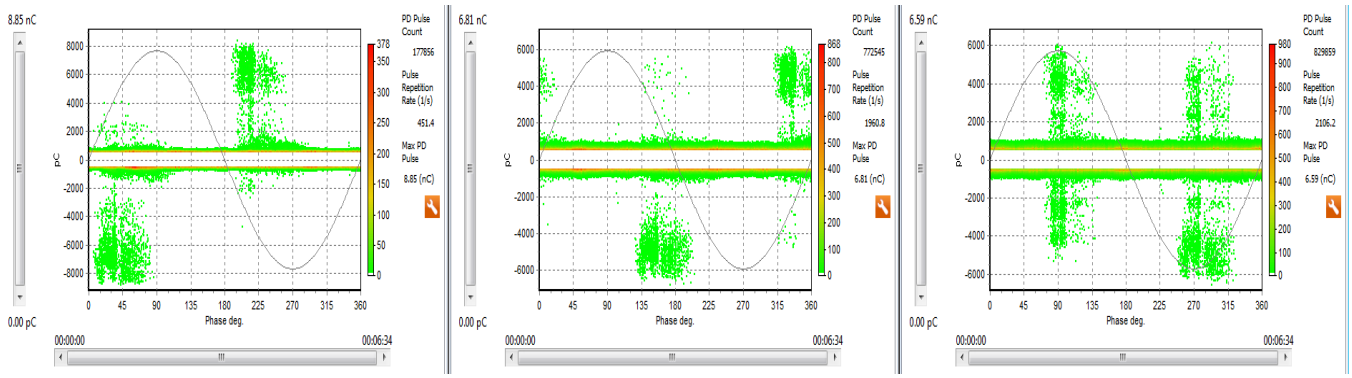

Fig.35. PRPD pattern recorded on CT4 (TB) with defect at CT (TB).

4.5 CONCLUSIONS

- The attenuation of the Higher frequency components of a PD pulse has been demonstrated through this research
- The utilization of the HF resonant components in the measured PD pulse allow a greater SNR but do not provide real value of charge.
- Applicability of the IEC 60270 measurement standards are relevant only while creating the test arrangement but bear no correlation while performing on-line measurements. Because calibration at frequencies lower than 100 kHz brings in very high levels of noise.

5 Dissemination Planning

As a result of this research, an abstract has already been submitted for the CIRED 2019 conference in Madrid, Spain.

Further analysis of the research resulting from this TA in conjunction with the host organization research could be developed for journal publication but this is to be confirmed.

A workshop for industrial organizations was held presenting research in progress during TA, promoting not only the research in itself but also the other host institutions available under the ERIGrid project.

6 References

[1] EC Joint Research Centre (JRC) publication, December 2014, "Towards an Integrated Roadmap: Research Innovation Challenges and Needs of the EU Energy System", available online http://setis.ec.europa.eu/system/files/Towards-an-Integrated-Roadmap_0.pdf

[2] P. Mulroy et al, ñOn-line Partial Discharge Monitoring System for Distribution Networksò, Condition Monitoring and Diagnosis (CMD), 2012 International Conference on, pp.542-545.

[3] L. Renforth et al, ñDeployment of distributed on-line partial discharge monitoring devices on medium voltage electricity networksò, Electricity Distribution - Part 1, 2009. CIRED 2009. 20th International Conference and Exhibition on, pp.1-4.

[4] M. Baier et al, 2009, ñPartial Discharge Online Measurements with Continuous Monitoring as Invaluable Tool for Assessing Insulation Quality and Maintenance Planningò, Proceedings CIRED 2009, 20th International Conference on Electricity Distribution, pp.1-4.

[5] P. Morshuis et al, ñPartial Discharge Diagnsotics ï Critical Steps towards On-line Monitoringò, T&D Conference and Exposition, 2014 IEEE PES, pp.1-5

[6] IEC 60270: Partial discharge measurement

[7] Cigré Technical Guide 444 ñGuidelines for Unconventional Partial Discharge Measurementsò

7 Annex

7.1 List of Figures